EUROPEAN ORGANIZATION FOR NUCLEAR RESEARCH

CERN/PPE 91-93
4 June 1991

STUDY OF THE $\eta\pi^+\pi^-$ SYSTEM CENTRALLY PRODUCED IN THE REACTION $pp \to p_f(\eta\pi^+\pi^-)p_s$ AT 300 GeV/c

WA76 Collaboration

Athens-Bari-Birmingham-CERN-Collège de France

T.A. Armstrong[4a], R.P. Barnes[3], M. Benayoun[5], W. Beusch[4], I.J. Bloodworth[3], J.N. Carney[3], D. Di Bari[2], C.J. Dodenhoff[3], D. Evans[3], B.R. French[4], B. Ghidini[2], M. Girone[2], A. Jacholkowski[4], J.B. Kinson[3], A. Kirk[4], K. Knudson[4], V. Lenti[2], V. Manzari[2], F. Navach[2], A. Palano[2], E. Quercigh[4], M. Sené[5], R. Sené[5], G. Vassiliadis[1], O. Villalobos Baillie[3], M.F. Votruba[3]

Abstract

The reaction $pp \to p_f(\eta\pi^+\pi^-)p_s$ where the $\eta\pi^+\pi^-$ system is centrally produced has been studied at 300 GeV/c incident momentum at the CERN Ω spectrometer. The $\eta\pi^\pm$ mass spectrum shows a strong $\delta/a_0(980)$ signal having a mass of 984±4 and Γ=95±14 MeV. The $\eta\pi^+\pi^-$ mass spectrum shows η' and $f_1(1285)$ signals over little background. A spin-parity analysis of the $\eta\pi^+\pi^-$ system shows evidence for a $J^{PC} = 1^{++}$ peak at the $f_1(1285)$ mass but no evidence for the pseudoscalar states $\eta(1270)$ and $\iota/\eta(1440)$. No evidence is found for the $\eta\pi\pi$ decay of the $E/f_1(1420)$ meson for which we set an upper limit $B.R.(E/f_1(1420) \to \eta\pi\pi) < 0.1$ at 95% c.l.

Submitted to Zeitschrift für Physik C

1) Athens University, Nuclear Physics Department, Athens, Greece
2) Dipartimento di Fisica dell'Università and Sezione INFN, Bari, Italy
3) University of Birmingham, Physics Department, Birmingham, U.K.
4) CERN, European Organization for Nuclear Research, Geneva, Switzerland
5) Collège de France, Paris, France
a) Present address: Pennsylvania State University, University Park, USA

1. INTRODUCTION

The mass region from 1.0 to 1.5 GeV has been extensively explored, during the last years, in order to search for mesonic resonances decaying to $K\bar{K}\pi$, $\eta\pi\pi$, 4π and $\rho\gamma$. The interest is due to the possible presence, in this mass region, of non $q\bar{q}$ mesons like glueballs, hybrids and $K\bar{K}$ molecules. The situation,however, is rather complex with several resonances being observed in this mass region which in some experiments have $J^{PC} = 0^{-+}$ and in others $J^{PC} = 1^{++}$ [1]. It is now clear that no single experiment can discover gluonium states and that the evidence for non $q\bar{q}$ mesons can only come from the comparison of light meson spectroscopy from several dynamical sources, i.e. J/ψ radiative and hadronic decay, π or K induced peripheral reactions, $p\bar{p}$ annihilation, $\gamma\gamma$ collisions and central production.

The $\eta\pi\pi$ system has been extensively analyzed, in the last few years, in most of the above processes. The study of radiative J/ψ decay to $K\bar{K}\pi$ has led to the discovery of a new resonance, the $\iota/\eta(1440)$ [2] having an important $\delta/a_0(980)\pi$ decay mode contribution. The absence of an $\iota/\eta(1440)$ signal in the radiative J/ψ decay to $\eta\pi\pi$ has been, for several years, a source of concern [3]. Recently, Partial Wave Analyses of the $K\bar{K}\pi$ and $\eta\pi\pi$ systems produced in radiative J/ψ decay [4,5] have indicated that the $\iota/\eta(1440)$ structure may be due to a mixture of several $J^{PC} = 0^{-+}$ and 1^{++} resonances whose classification in the quark model is still unclear.

Another relevant problem in meson spectroscopy is the nature of the $E/f_1(1420)$ meson, a $J^{PC} = 1^{++}$ state up to now observed to decay only to $K^*\bar{K}$, a fact which suggests a dominant $s\bar{s}$ component in its wavefunction. The $E/f_1(1420)$ has been observed in central production from hadron hadron interactions [6] and in $\gamma\gamma$ collisions [7]. However, this state is not produced in incident K^- reactions [8], where a different $J^{PC} = 1^{++}$ state is observed, the $f_1(1520)$, which has the expected properties of the $s\bar{s}$ member of the $J^{PC} = 1^{++}$ nonet. The $E/f_1(1420)$ is then left out from this multiplet and is a candidate for being a hybrid $(u\bar{u} + d\bar{d})g$ state [9], a $K^*\bar{K}$ molecule or a 4-quark state [10].

The 1.0 to 2.0 GeV region is also predicted [11] to be densely populated with radial excitations of the ground state multiplets, a fact which complicates the search for extra states beyond the quark model. For example, Partial Wave Analysis of the $\eta\pi\pi$ system in the reaction $\pi^- p \to \eta\pi\pi n$ [12] provides evidence for the $f_1(1285)$ and two pseudoscalar states, $\eta(1275)$ and $\eta(1390)$, which have been interpreted as radial excitations of the $J^{PC} = 0^{-+}$ multiplet. However, the study of the $\eta\pi\pi$ system in $\gamma\gamma$ collisions, where radial excitations are expected to appear, does not show evidence for these resonances [13]. On the other hand, the study of $\gamma\gamma^* \to \eta\pi\pi$ shows evidence for production of $f_1(1285)$ but not of $E/f_1(1420)$.

Further information comes from J/ψ decay where its radiative decay to $\eta\pi\pi$ shows evidence for $f_1(1285)$ and for a pseudoscalar state in the 1.4 GeV region [5] while J/ψ hadronic decay to $\omega\eta\pi\pi$ shows evidence for structures in the 1.28 GeV and 1.42 GeV mass regions [14].

Thus all the above results show that this mass region is complicated. In order to contribute to the understanding of light meson spectroscopy and search for non $q\bar{q}$ mesons,

we have performed a systematic study of exclusive resonance production in the central region of hadron-hadron scattering. The study of the centrally produced $K^0_S K^{\pm}\pi^{\mp}$ final state in p p collisions at 300 GeV/c has shown production of $f_1(1285)$ and $E/f_1(1420)$ [6]. It is therefore of interest to search, in the same experiment, for an $\eta\pi\pi$ decay mode of these resonances.

The data come from the WA76 experiment performed at the CERN Omega spectrometer. Details on trigger conditions and data processing can be found in previous publications [15].

2. SELECTION OF THE REACTION $pp \to p_f(\pi^+\pi^-\eta_{\to\gamma\gamma})p_s$

The reaction

$$pp \to p_f(\pi^+\pi^-\eta_{\to\gamma\gamma})p_s \tag{1}$$

where the symbols f and s refer to the fast and slow proton respectively, has been selected from the sample of 4 prong events having only two reconstructed γ's each having an energy greater than 2 GeV reconstructed in the electromagnetic calorimeters (PLUG [16] and GPD [17]). Showers in the calorimeters associated to charged tracks have been removed. In order to remove soft photons associated with the fast track the energy cut has been raised to 2.5 GeV in a region having 30 cm radius in the central part of the electromagnetic calorimeter.

Momentum balancing events were selected by requiring |missing Px| < 30 GeV/c, | missing Py| < 0.2 GeV/c and |missing Pz| < 0.1 GeV/c. Energy balance was obtained by requiring the Ehrlich mass squared (m^2_X) [18,19], computed for the two charged tracks, to be $|m^2_X| < 0.2$ GeV^2. Fig. 1 shows the $\gamma\gamma$ effective mass for the selected sample where clear peaks corresponding to π^0 and η can be seen. Reaction (1) has been selected by requiring 0.48 GeV $< m(\gamma\gamma) <$ 0.64 GeV. The momenta of the two γ's have been constrainted in order to give the η mass. Diffractive contributions have been antiselected by requiring the centre of mass rapidities of the π^+ and η to be less than 1.7 and 2.0 respectively. These cuts remove a small Δ^{++} signal observed in the $p_f\pi^+$ effective mass distribution and a threshold enhancement observed in the $p_f\eta$ effective mass distribution. The final sample consists of 1582 events for which the $\eta\pi^+\pi^-$ effective mass distribution is shown in fig. 2.

We observe clear peaks at the $\eta'(975)$ and $f_1(1285)$ masses and no evidence for structure in the E/ι region.

3. SELECTION OF THE REACTION $pp \to p_f(\pi^+\pi^-\eta_{\to\pi^+\pi^-\pi^0})p_s$

The reaction

$$pp \to p_f(\pi^+\pi^-\eta_{\to\pi^+\pi^-\pi^0})p_s \tag{2}$$

has been selected from the sample of 6 prong events having only two reconstructed γ's each with an energy greater than 1 GeV deposited in the electromagnetic calorimeters.

Momentum balancing events were selected by requiring |missing Px| < 30 GeV/c, |missing Py| < 0.2 GeV/c and |missing Pz| < 0.1 GeV/c. Energy balance was obtained by requiring the function Δ, defined as

$$\Delta = mm^2(p_f p_s) - m^2(2\pi^+ 2\pi^- 2\gamma)$$

where mm^2 is the missing mass squared to the $p_f p_s$ system, to be $|\Delta| < 4.0$ GeV^2.

The $\gamma\gamma$ effective mass distribution is shown in fig. 3(a) where a clear π^0 peak over a small background can be seen. The π^0 signal has been selected by requiring $0.096 < m(\gamma\gamma) < 0.174$ GeV. The momenta of the two γ's have been constrainted to give the π^0 mass. The $p_f\pi^0$ effective mass distribution (not shown) shows evidence for Δ^+ production which has been removed by requiring the centre of mass rapidity of the π^0 to be less than 2.1. Fig. 3(b) shows the $\pi^+\pi^-\pi^0$ effective mass distribution (4 combinations per event). The $\eta(548)$ and $\omega(783)$ signals can be seen, showing evidence for the centrally produced $\eta\pi^+\pi^-$ and $\omega\pi^+\pi^-$ final states respectively. Reaction (2) has then been isolated by keeping the $\pi^+\pi^-\pi^0$ mass combination closest to the η mass and requiring that $0.535 < m(\pi^+\pi^-\pi^0) < 0.565$ GeV. The momenta of the three pions in the η region have been summed and the energy has been recomputed using the η mass. The selected sample consists of 469 events whose $\eta\pi^+\pi^-$ effective mass spectrum is shown in fig. 4. The spectrum is similar to that obtained in fig. 2 for the $\eta \to \gamma\gamma$ decay mode.

4. STUDY OF THE MASS SPECTRA

The combined $\eta\pi^+\pi^-$ mass spectrum for reactions (1) and (2) is shown in fig. 5. Fig. 6(a,b) shows the $\eta\pi^\pm$ and $\pi^+\pi^-$ effective mass distributions after having removed the η' region (i.e. $m_{\eta\pi\pi} < 1.1$ GeV). The $\eta\pi^\pm$ mass spectrum shows a strong $\delta/a_0(980)$ along with some $a_2(1320)$, while the $\pi^+\pi^-$ mass distribution does not show evidence for $\rho^0(770)$. The Feynman x_F distributions for the slow proton, the central $\eta\pi^+\pi^-$ system and the fast proton are shown in fig. 7.

A fit has been performed to the combined $\eta\pi^+\pi^-$ mass spectrum of fig. 5, using a Gaussian to describe the η' region and a Breit-Wigner convoluted with a Gaussian to describe the $f_1(1285)$ region. The $f_1(1285)$ width has been fixed to the PDG value (Γ=25 MeV) [20]. The σ of the Gaussians have been left as free parameters in order to obtain the experimental resolutions. The results of the fit are

$$\begin{aligned} m_{\eta'} &= 958 \pm 1 \quad \text{MeV} \quad , \\ \sigma_{\eta'} &= 8 \pm 1 \quad \text{MeV} \quad , \\ m_{f_1(1285)} &= 1282 \pm 2 \quad \text{MeV} \quad , \\ \sigma_{f_1(1285)} &= 19 \pm 2 \quad \text{MeV} \quad . \end{aligned}$$

In order to obtain a description of the $\eta\pi^\pm$ effective mass and measure the $\delta/a_0(980)$ parameters we have fitted the combined $\eta\pi^\pm$ mass spectrum shown in fig. 6(a). The

$\delta/a_0(980)$ has been described by a relativistic S-wave Breit-Wigner convoluted with a Gaussian having a σ=20 MeV; the $a_2(1320)$ has been described by a relativistic spin-2 Breit-Wigner having parameters fixed to the PDG values. The result from the fit is shown in fig. 6(a) and gives the following parameters for the $\delta/a_0(980)$

$$m(a_0) = 984 \pm 4 \quad \text{MeV} \quad ,$$
$$\Gamma(a_0) = 95 \pm 14 \quad \text{MeV} \quad .$$

In order to study the correlation between the $\eta\pi^+\pi^-$ system and the resonances observed in the $\eta\pi^\pm$ system we have plotted in fig. 8 the scatter plot m($\eta\pi^\pm$) vs. m($\eta\pi^+\pi^-$) (2 combinations per event). A clear correlation can be seen between $\delta/a_0(980)$ and the $f_1(1285)$ signal while the vertical band in the $f_1(1285)$ region is due to the fact that when one $\eta\pi$ combination falls in the $\delta/a_0(980)$, the other falls below. Requiring either $\eta\pi$ combination to be in the δ region ($0.88 < \text{m}(\eta\pi) < 1.08$ GeV), we obtain the $\delta\pi$ mass spectrum shown in fig. 9(a) where the $f_1(1285)$ can be seen. The $a_2(1320)\pi$ mass spectrum is shown in fig. 9(b), where the $a_2(1320)$ region is defined as $1.20 < \text{m}(\eta\pi) < 1.42$ GeV. No evidence is seen for the new resonance X(1900) recently observed in the reaction $\gamma\gamma \rightarrow \eta\pi\pi$ [21].

5. SPIN PARITY ANALYSIS OF THE $\eta\pi^+\pi^-$ SYSTEM

A mass dependent spin parity analysis of the $\eta\pi^+\pi^-$ system has been performed in order to establish the nature of the structure observed in the 1.28 GeV region and search for other resonances.

Fits were performed on the Dalitz plot of the $\eta\pi\pi$ system using the Zemach tensor formalism [22]. An isobar model is used assuming the $\delta/a_0(980)\pi$, $\epsilon/f_0(1400)\eta$ and $\rho(770)\eta$ intermediate states. The $\epsilon/f_0(1400)$ has been parameterized as a $\pi\pi$ phase shift [23] or a broad Breit-Wigner. These different parameterizations do not affect the results of the spin parity analysis significantly. Since the spin analysis has been performed only up to an $\eta\pi\pi$ mass of 1.6 GeV, higher spin isobars $a_2(1320)\pi$ or $f_2(1270)\eta$ have been ignored. Waves up to spin 1 have been considered in this mass range. Interference was allowed between waves having the same spin-parity. The list of the tensors used in this analysis is given in table I.

The geometrical acceptance of the apparatus for reactions (1) and (2) has been evaluated as a function of the $\eta\pi\pi$ effective mass and over the Dalitz plot. We found that the data are not distorted by the geometrical acceptance of the apparatus, so that the analysis has been performed without corrections. In the spin analysis we used the combined data samples from reactions (1) and (2). The fits have been performed by maximum likelihood dividing the data into slices of 50 MeV as a function of the $\eta\pi\pi$ effective mass. Waves having small statistical significance have been removed from the fit.

The results are shown in fig. 10 and can be summarized as follows:

(a) The $J^{PC} = 1^{++}$ $\delta/a_0(980)\pi$ is the dominant wave and peaks at the $f_1(1285)$ mass. No evidence is seen for other resonant states; in particular, no evidence is seen for $E/f_1(1420)$ production. This confirms the results from the spin analysis of the centrally produced $K^0_S K^{\pm}\pi^{\mp}$ system [6] which gave a $\delta\pi$ contribution consistent with zero in the $E/f_1(1420)$ region.

(b) The $J^{PC} = 0^{-+}$ waves are small and do not show resonant behaviour. In particular, no evidence is seen for $\eta(1270)$ or the pseudoscalar states observed in radiative J/ψ decay.

(c) There is no evidence for $\rho'(1450) \rightarrow \eta\rho(770)$ suggested by the study of the $\eta\pi\pi$ system from incident π^- [24]. This is not unexpected since the production of ρ-like resonances in the central region decreases with the increasing centre of mass energy [19].

The Dalitz plot of the $f_1(1285)$ region (1.20 - 1.36 GeV, 626 events) is shown in fig. 11 together with Monte-Carlo simulations of pure $J^{PC} = 0^{-+}$ and 1^{++} $\delta/a_0(980)\pi$ waves computed at the $f_1(1285)$ mass.

6. COMPARISON WITH THE $K^0_S K^{\pm}\pi^{\mp}$ CHANNEL

In order to have more information on the properties of the $E/f_1(1420)$ meson we have compared the results obtained from the analysis of the $\eta\pi\pi$ system with those obtained from the study of the $K^0_S K^{\pm}\pi^{\mp}$ system in the reaction

$$pp \rightarrow p_f(K^{\pm}K^0_S\pi^{\mp})p_s \qquad (3)$$

Details on the selection of reaction (3) have been given in ref. [6]. The mass spectrum is shown in fig. 12 where clear signals corresponding to $f_1(1285)$ and $E/f_1(1420)$ can be seen. In order to compute the upper limit for the production of $E/f_1(1420)$ in the $\eta\pi\pi$ final state we have fitted the mass spectrum shown in fig. 5 without including that region and using the interpolated background to obtain an upper limit on the $E/f_1(1420)$ yield. Taking as reference the presence of the $f_1(1285)$ in both the $\eta\pi\pi$ and $K^0_S K^{\pm}\pi^{\mp}$ mass spectra, and assuming an $f_1(1285)$ branching ratio to $K\bar{K}\pi$ of 12 % [20], we measure an upper limit for the decay of $E/f_1(1420)$ to $\eta\pi\pi$

$$B.R.(E/f_1(1420) \rightarrow \eta\pi\pi) < 0.1 \quad 95\% c.l.$$

This is in contradiction with the large branching ratio found for $E/f_1(1420) \rightarrow \eta\pi\pi$ observed recoiling against the ω in the reaction $J/\psi \rightarrow \omega\eta\pi\pi$ [14]. This result is particularly relevant in establishing the $E/f_1(1420)$ meson properties. The decay pattern observed in hadronic J/ψ decay to $\phi K\bar{K}\pi$ and $\omega K\bar{K}\pi$ [14] indicates a substantial $u\bar{u}$ and $d\bar{d}$ quark composition of the $E/f_1(1420)$ meson which would lead one to expect $\eta\pi\pi$ or 4π decay modes. However, this expectation is in contradiction with the non observation of the $E/f_1(1420)$ decay to other than the $K^*\bar{K}$ mode [25].

7. STUDY OF THE t DEPENDENCE

Assuming the resonances observed in the present experiment to be produced by a double exchange graph as shown in fig. 13, we have divided the $\eta\pi\pi$ and $K^{\pm}K^{0}_{S}\pi^{\mp}$ mass spectra in two samples, i.e. $t < 0.3$ GeV^2 and $t > 0.3$ GeV^2 (where $t = t_1 + t_2$). The mass spectra corresponding to these selections are shown in fig. 14. We observe a depletion of the η' signal in the low t region.

In order to measure the t dependence of the observed resonances, we have divided the data into four slices of t and then computed the geometrical acceptance of the apparatus as a function of t. The corrected and uncorrected t distributions for η' and $f_1(1285)$, from the $\eta\pi\pi$ channel, are shown in fig. 15(a,b). We observe that, while for the η' the distribution shows a depletion at low t, the $f_1(1285)$ distribution is consistent with a simple exponential $exp(-bt)$ with $b = 6.5 \pm 0.4$ GeV^{-2}. The results from the same analysis performed on the $K^{\pm}K^{0}_{S}\pi^{\mp}$ data are shown in fig. 15(b,c) for $f_1(1285)$ and $E/f_1(1420)$ respectively. We observe that the $f_1(1285)$ has a simple exponential behaviour with a slope $b = 7.3 \pm 0.7$ GeV^{-2} consistent with that obtained from the study of the $\eta\pi\pi$ channel.

8. CONCLUSIONS

The reaction $pp \to p_f(\eta\pi^+\pi^-)p_s$ where the $\eta\pi^+\pi^-$ system is centrally produced has been studied at 300 GeV/c incident momentum. The $\eta\pi^{\pm}$ mass spectrum shows a strong $\delta/a_0(980)$ signal having a mass of 984±r4 and Γ=95±14 MeV. The $\eta\pi^+\pi^-$ mass spectrum shows η' and $f_1(1285)$ signals over little background. A spin-parity analysis of the $\eta\pi^+\pi^-$ system shows evidence for a $J^{PC} = 1^{++}$ peak at the $f_1(1285)$ mass but no evidence for the pseudoscalar states $\eta(1270)$ and $\iota/\eta(1440)$. No evidence is found for the $\eta\pi\pi$ decay of the $E/f_1(1420)$ meson for which we set an upper limit $B.R.(E/f_1(1420) \to \eta\pi\pi) < 0.1$ at 95% c.l.

ACKNOWLEDGMENTS

We acknowledge D. Caldwell, Ph. Gavillet and A. Seiden for useful discussions.

REFERENCES

[1] A.Palano, Proc. of the Hadronic Session of the XXII Rencontre de Moriond (1987), Ed. Frontiéres.

[2] D.L. Scharre et al., Phys. Lett. 97B (1980) 329;

C. Edwards et al., Phys. Rev. Lett. 49 (1982) 259.

[3] M. Frank et al., Phys. Lett. 158B (1985) 442.

[4] Z. Bai et al., Phys. Rev. Lett. 65 (1990) 2507.

J.J. Drinkard, SCIPP 90/16, May 1990.

[5] J.E. Augustin et al., Phys. Rev. D42 (1990) 10.

J.E. Augustin et al., LAL 90-70 November 1990.

[6] T. A. Armstrong et al., Phys. Lett. 146B (1984) 273;

T. A. Armstrong et al., Z. Phys. C34 (1987) 23;

T. A. Armstrong et al., Phys. Lett. 221B (1989) 216.

[7] H. Aihara et al., Phys. Rev. Lett. 57 (1986) 2500;

G. Gidal et al., Phys. Rev. Lett. 59 (1987) 2016;

[8] Ph. Gavillet et al., Z. Phys. C16 (1982) 119;

D. Aston et al., Phys. Lett. 201B (1988) 573.

[9] S. Ishida et al., Progress of Theoretical Phys. 82 (1989) 119

[10] D.O. Caldwell, Mod. Phys. Lett. A2 (1987) 771;

R.S. Longacre, Phys. Rev. D42 (1990) 874.

[11] S. Godfrey and N. Isgur, Phys. Rev. D32 (1985) 189.

[12] N.R. Stanton et al., Phys. Rev. Lett. 42 (1979) 346;

A. Ando et al., Phys. Rev. Lett., 57 (1986) 1296.

[13] G. Gidal et al., Phys. Rev. Lett. 59 (1987) 2012.

[14] L. Köpke and N. Wermes, Phys. Rep. 174 (1989) 67.

[15] T. A. Armstrong et al., Nucl. Instr. and Meth. A274 (1989) 165.

[16] H. Burmeister et al., Nucl. Instr. and Meth. A225 (1984) 530

[17] M. Bonesini et al., Nucl. Instr. and Meth. A261 (1987) 471.

[18] R. Ehrlich et al., Phys. Rev. Lett. 20 (1968) 686.

REFERENCES (Cont'd)

[19] T.A. Armstrong et al., CERN/PPE 91-40, 20 February 1991, to be published by Z. Phys. C.

[20] Review of Particles Properties, Phys. Lett. B239 (1990).

[21] K. Karch et al., Phys. Lett. B249 (1990) 353;

M. Feindt, DESY 90-128, October 1990.

[22] C. Zemach, Phys. Rev. 140, B97 (1965).

[23] B. Hyams et al., Nucl. Phys. B64 (1973) 134;

S. Protopopescu et al., Phys. Rev. D7 (1973) 1280.

[24] S. Fukui et al., Phys. Lett. B202 (1988) 441.

[25] T.A. Armstrong et al., Phys. Lett. B228 (1989) 536.

Table I

Decay amplitudes for $\delta\pi$, $\eta\varepsilon$ and $\eta\rho$ modes

J^P	L	Decay Modes	Amplitudes
0^-	0	$\delta\pi$	$BW(\delta^+_{12}) + BW(\delta^-_{13})$
1^+	1	$\delta\pi$	$BW(\delta^+_{12})\mathbf{p}_3 + BW(\delta^-_{13})\mathbf{p}_2$
0^-	0	$\eta\varepsilon$	$BW(\varepsilon_{23})$
1^+	1	$\eta\varepsilon$	$BW(\varepsilon_{23})\mathbf{p}_1$
1^+	0	$\eta\rho$	$BW(\rho^\circ_{23})\mathbf{q}_1$
0^-	1	$\eta\rho$	$BW(\rho^\circ_{23})\mathbf{q}_1 \cdot \mathbf{p}_1$
1^-	1	$\eta\rho$	$BW(\rho^\circ_{23})\mathbf{q}_1 \times \mathbf{p}_1$

$$X \rightarrow \eta_1 \pi^+_2 \pi^-_3$$

$\mathbf{p}_i$(i=1, 2, 3) are the vector parts of the three decaying particle 4-momenta in the X c.m. system

$\mathbf{q}_1 = \mathbf{p}_2 - \mathbf{p}_3$

FIGURE CAPTIONS

Fig. 1 $\gamma\gamma$ effective mass distribution for 4 prong events balancing momentum and having only two γ's reconstructed in the electromagnetic calorimeters. The inset shows the η region.

Fig. 2 $\eta\pi^+\pi^-$ effective mass distribution for the events where $\eta \to \gamma\gamma$.

Fig. 3 (a) $\gamma\gamma$ efective mass for 6 prong events having only two γ's reconstructed in the electromagnetic calorimeters.

(b) $\pi^+\pi^-\pi^0$ effective mass distribution (4 combinations per events) from the reaction $pp \to p_f(2\pi^+2\pi^-\pi^0)p_s$.

Fig. 4 $\eta\pi^+\pi^-$ effective mass distribution for the events where $\eta \to \pi^+\pi^-\pi^0$.

Fig. 5 Combined $\eta\pi^+\pi^-$ effective mass distribution for reactions (1) and (2). The Curve is the result from the fit described in the text. The inset shows the η' region.

Fig. 6 (a) $\eta\pi^\pm$ effective mass distribution. The curves are the results from the fit described in the text.

(b) $\pi^+\pi^-$ effective mass distribution.

Fig. 7 Feynman-x_F distribution for the slow proton, the $\eta\pi^+\pi^-$ system and the fast proton.

Fig. 8 Scatter diagram m($\eta\pi^\pm$) vs. m($\eta\pi^+\pi^-$).

Fig. 9 (a) $\delta\pi$ effective mass distribution; (b) $a_2\pi$ effective mass distribution.

Fig. 10 Results from the Dalitz plot analysis.

Fig. 11 The Dalitz plot for the $f_1(1285)$ region is compared with Monte-Carlo simulations for pure 0^{-+} and 1^{++} $\delta\pi$ computed at the $f_1(1285)$ mass.

Fig. 12 $K^0_S K^\mp\pi^\pm$ effective mass distribution from reaction (3).

Fig. 13 Double exchange graph for centrally produced $\eta\pi\pi$ and $K\bar{K}\pi$ systems.

Fig. 14 (a) $K^0_S K^\pm\pi^\mp$ effective mass for t < 0.3 GeV^2;

(b) $K^0_S K^\pm\pi^\mp$ effective mass for t > 0.3 GeV^2;

(c) $\eta\pi^+\pi^-$ effective mass for t < 0.3 GeV^2;

(d) $\eta\pi^+\pi^-$ effective mass for t > 0.3 GeV^2.

Fig. 15 1/t dN/dt distributions (in arbitrary units) for: (a) $\eta' \to \eta\pi\pi$; (b) $f_1(1285) \to \eta\pi\pi$; (c) $f_1(1285) \to K\bar{K}\pi$ and (d) $E/f_1(1420) \to K\bar{K}\pi$. Open points: uncorrected data; black points: data corrected by geometrical acceptance.

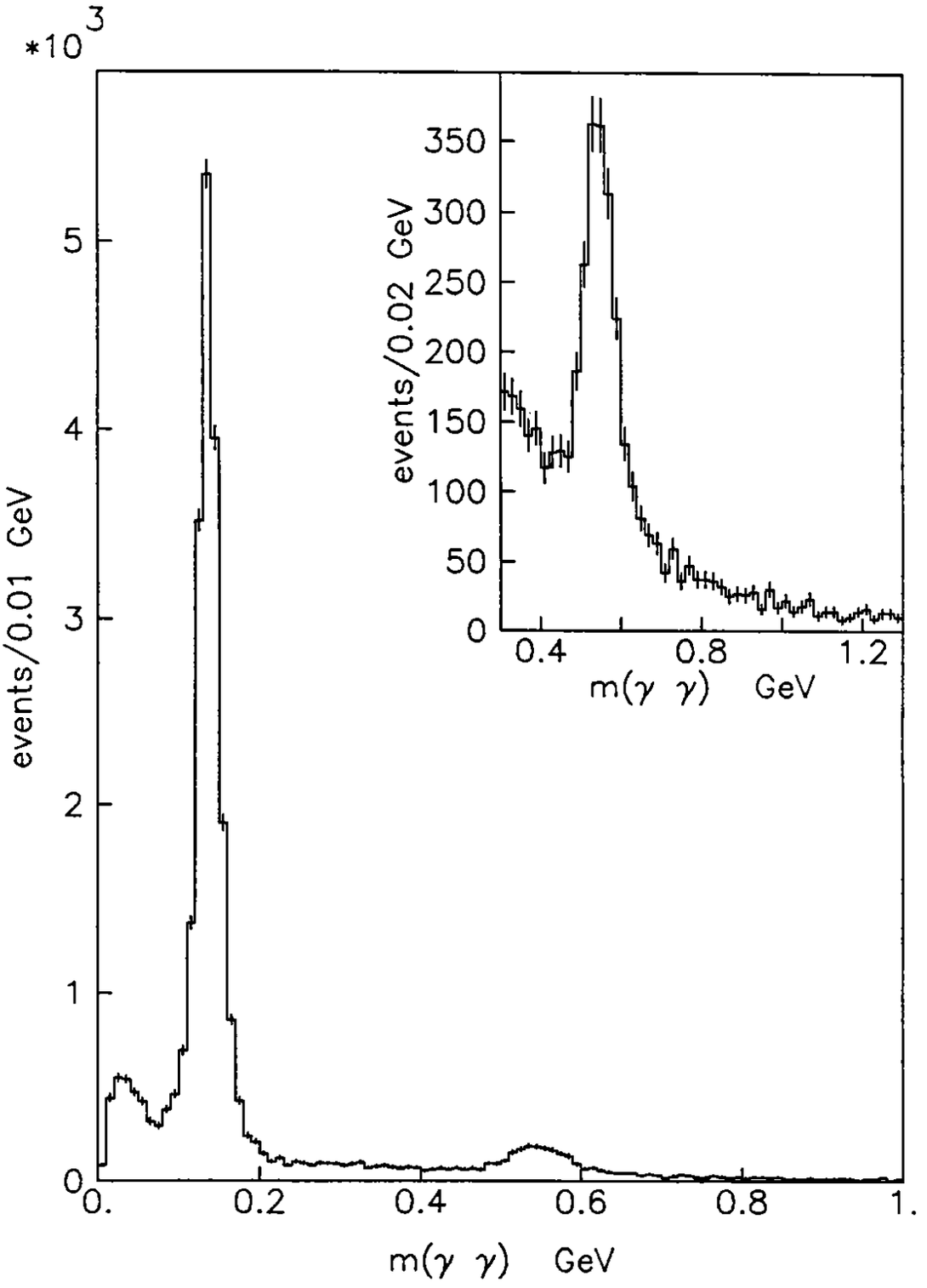

Fig. 1

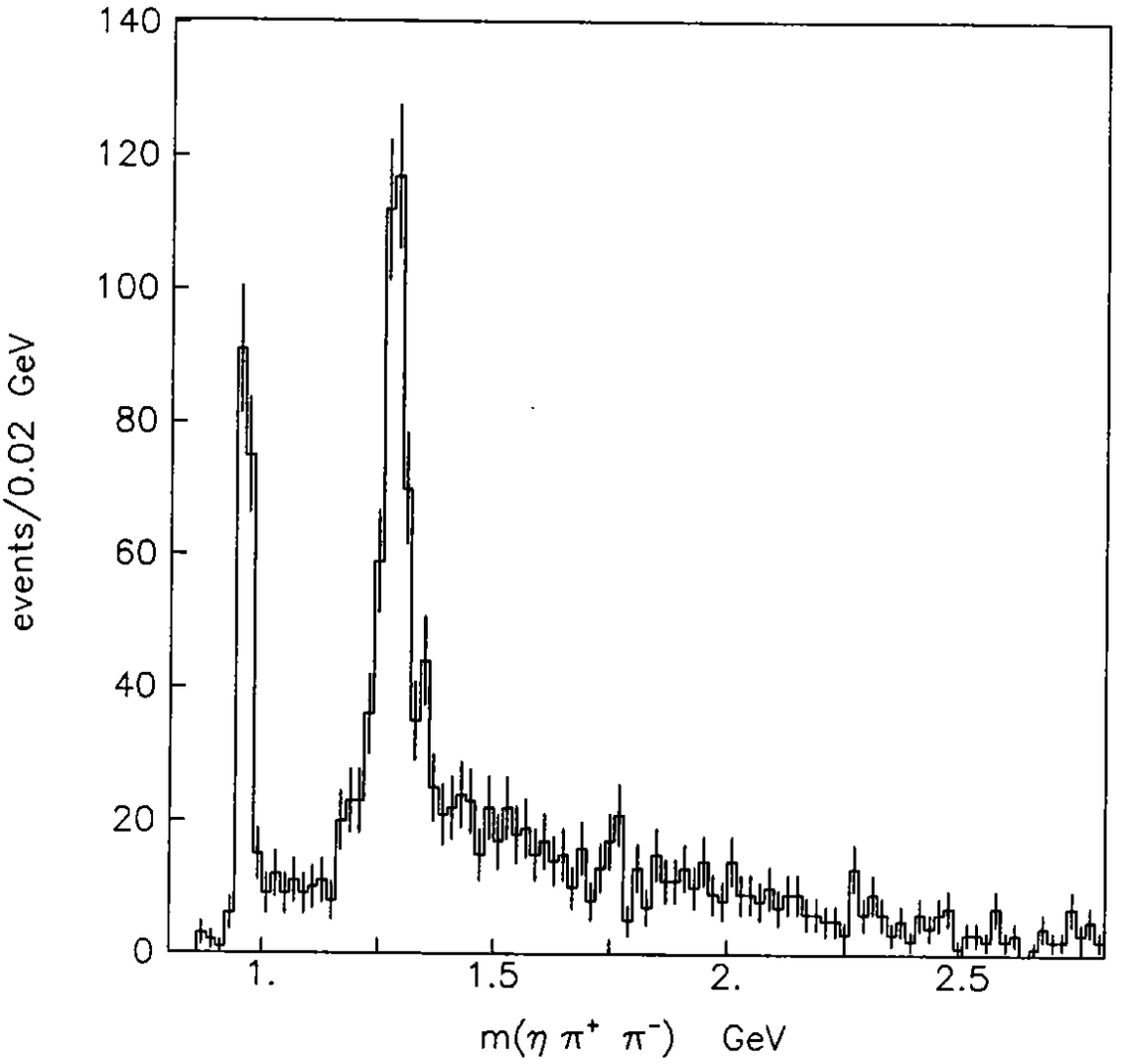

Fig. 2

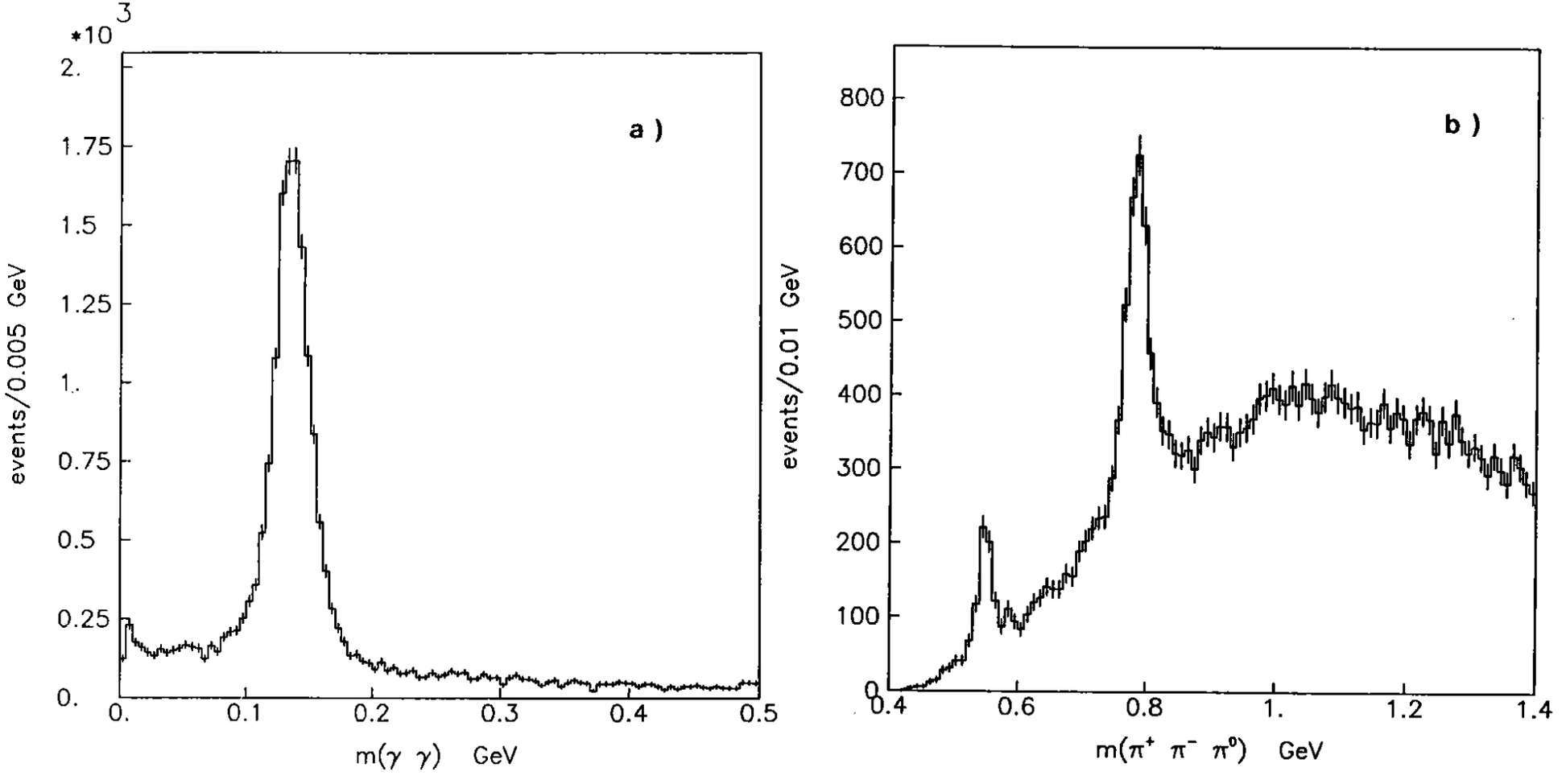
*10 3
2.
1.75
1.5
1.25
1.
0.75
0.5
0.25
0.
events/0.005 GeV
a)
0.
0.1
0.2
0.3
0.4
0.5
m(γ γ) GeV
events/0.01 GeV
800
700
600
500
400
300
200
100
0
b)
0.4
0.6
0.8
1.
1.2
1.4
m(π+ π− π0) GeV

Fig. 3

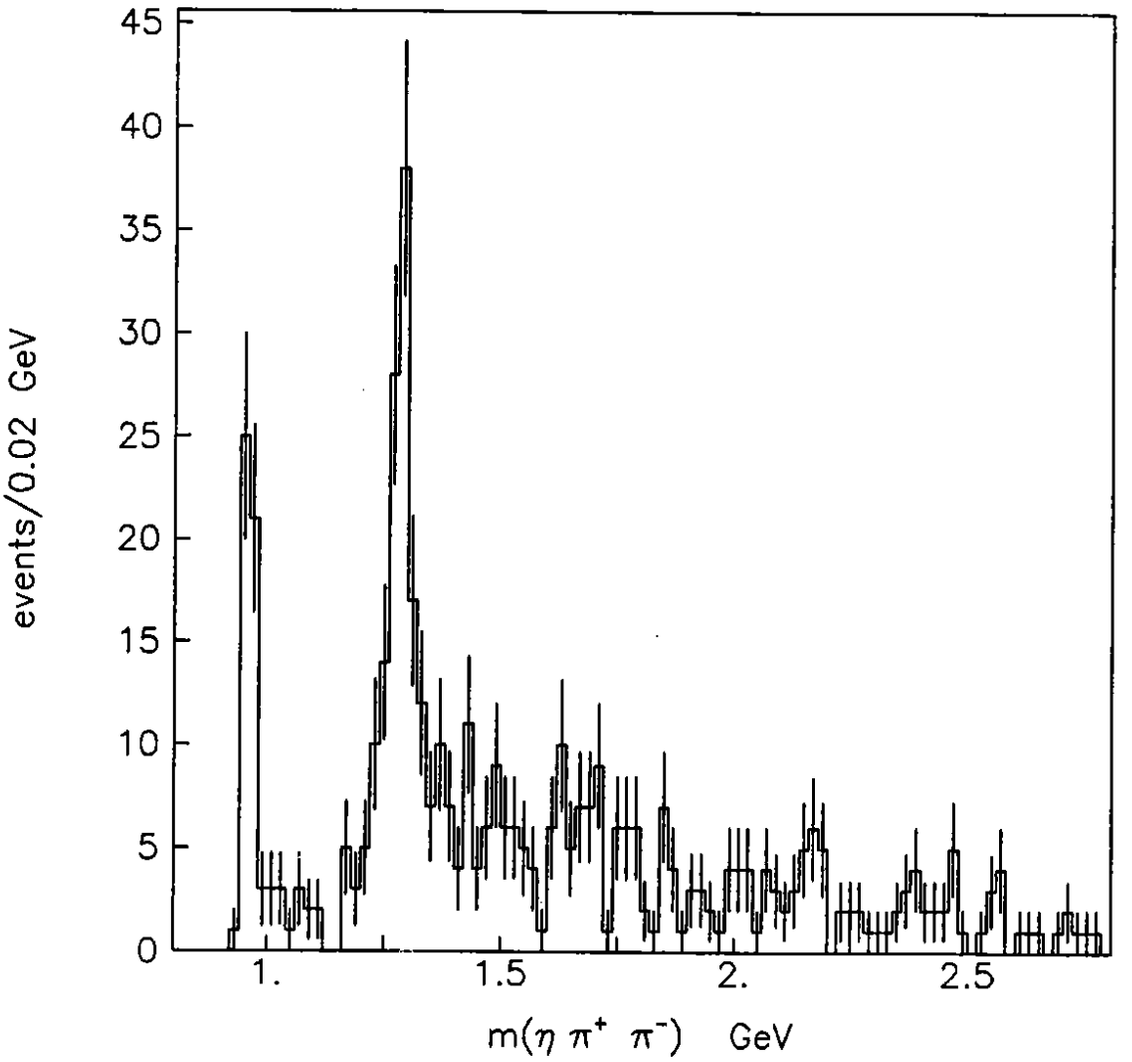

Fig. 4

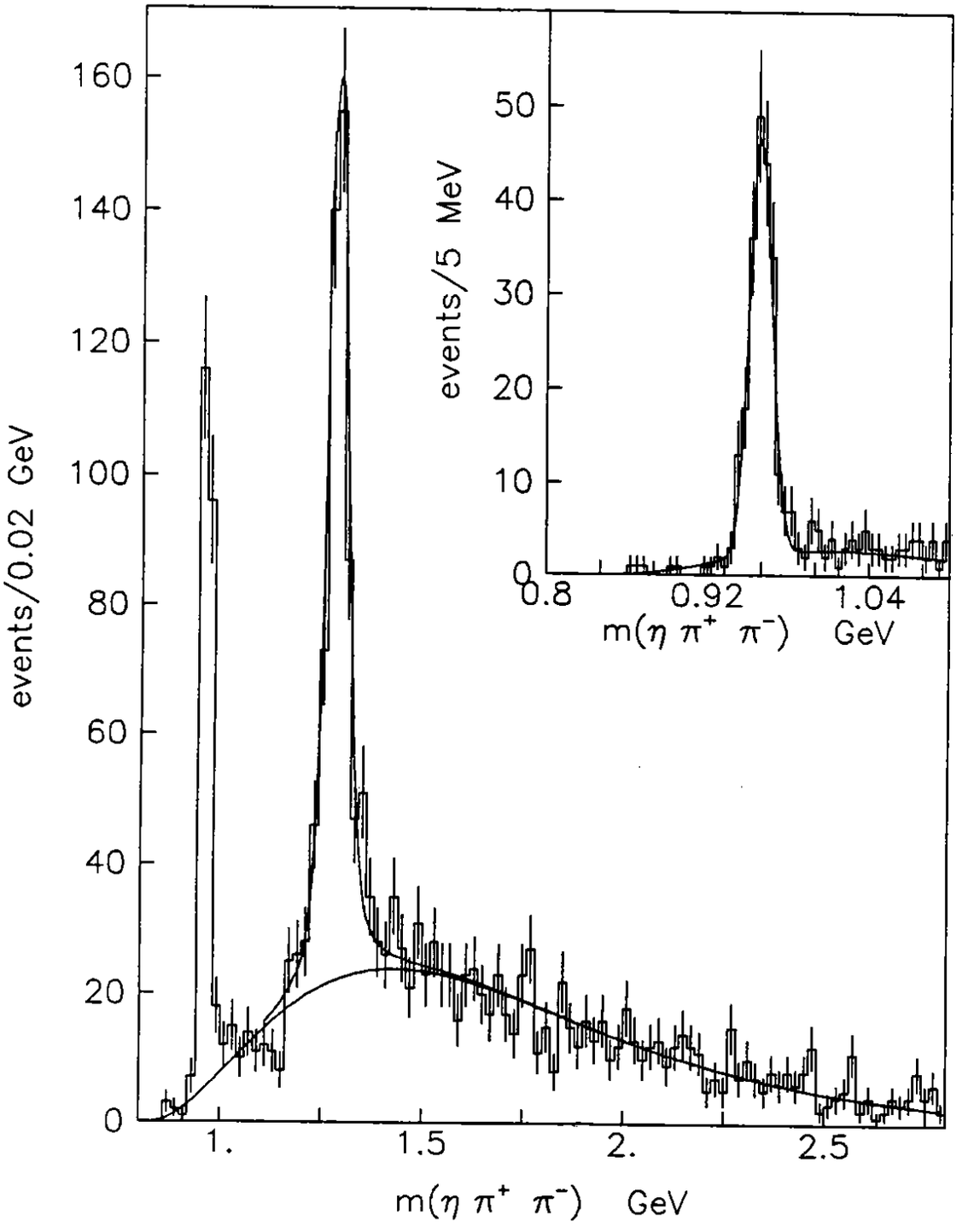
events/0.02 GeV
160
140
120
100
80
60
40
20
0
1.
1.5
2.
2.5
m(η π⁺ π⁻) GeV
events/5 MeV
50
40
30
20
10
0
0.8
0.92
1.04
m(η π⁺ π⁻) GeV

Fig. 5

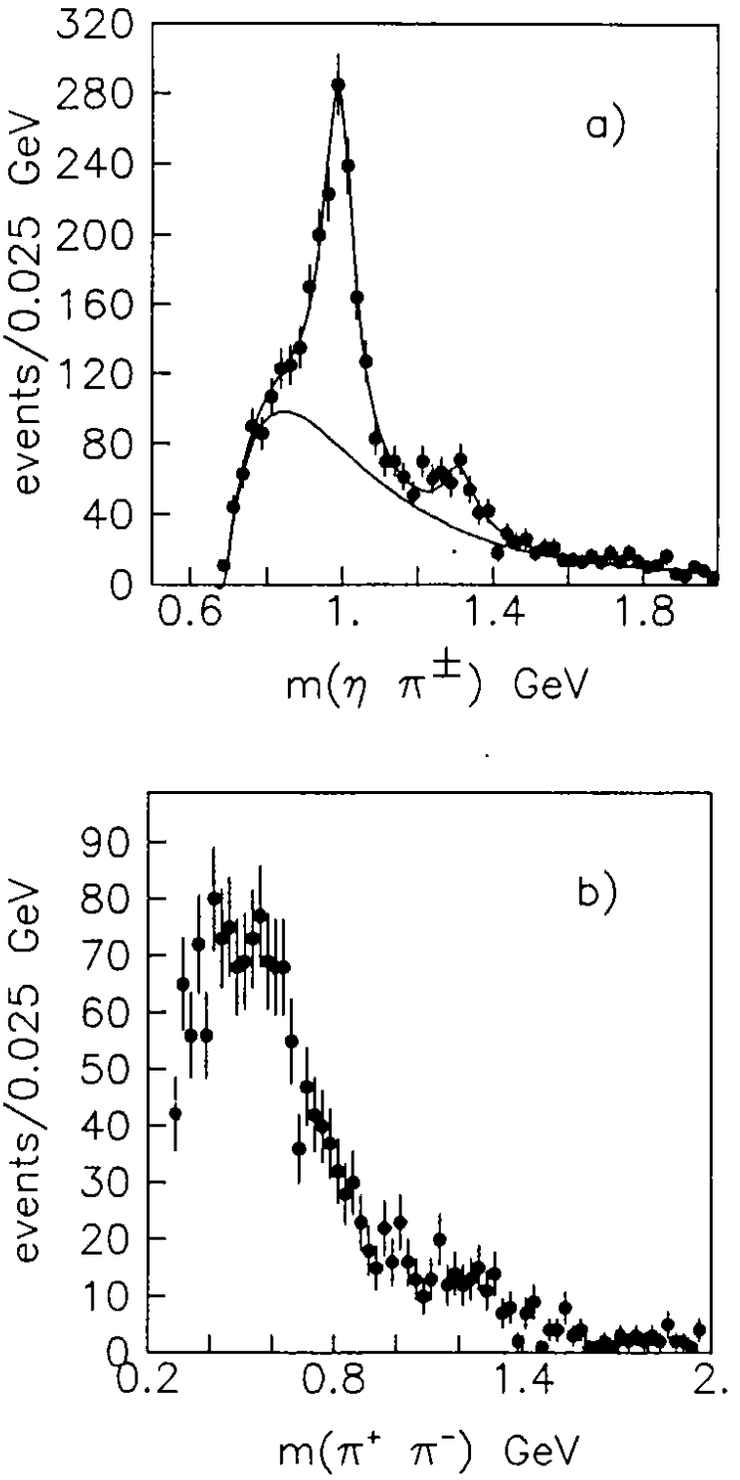
a)
events/0.025 GeV
320
280
240
200
160
120
80
40
0
0.6
1.
1.4
1.8
m(η π±) GeV
b)
events/0.025 GeV
90
80
70
60
50
40
30
20
10
0
0.2
0.8
1.4
2.
m(π+ π−) GeV

Fig. 6

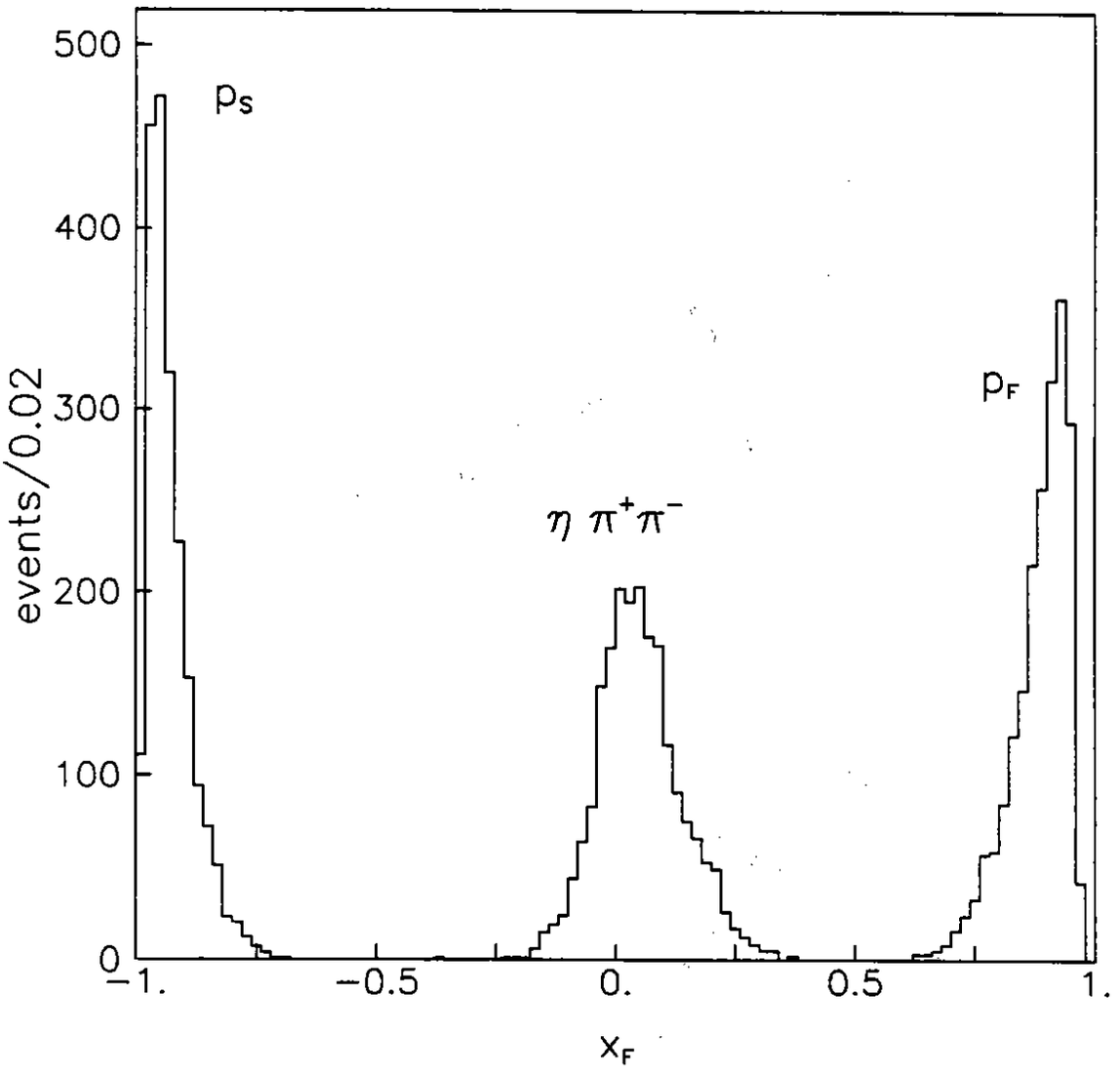

Fig. 7

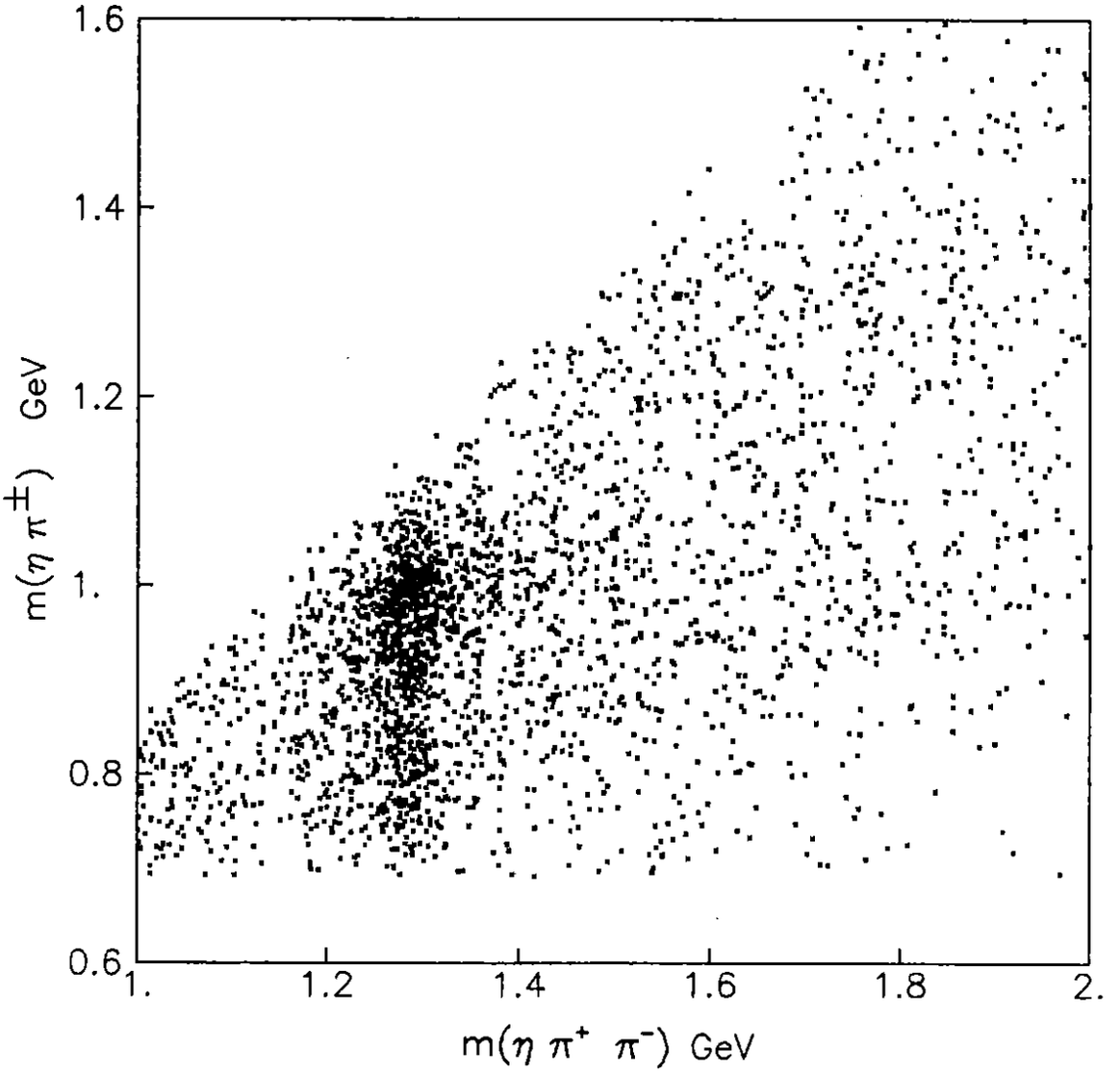

Fig. 8

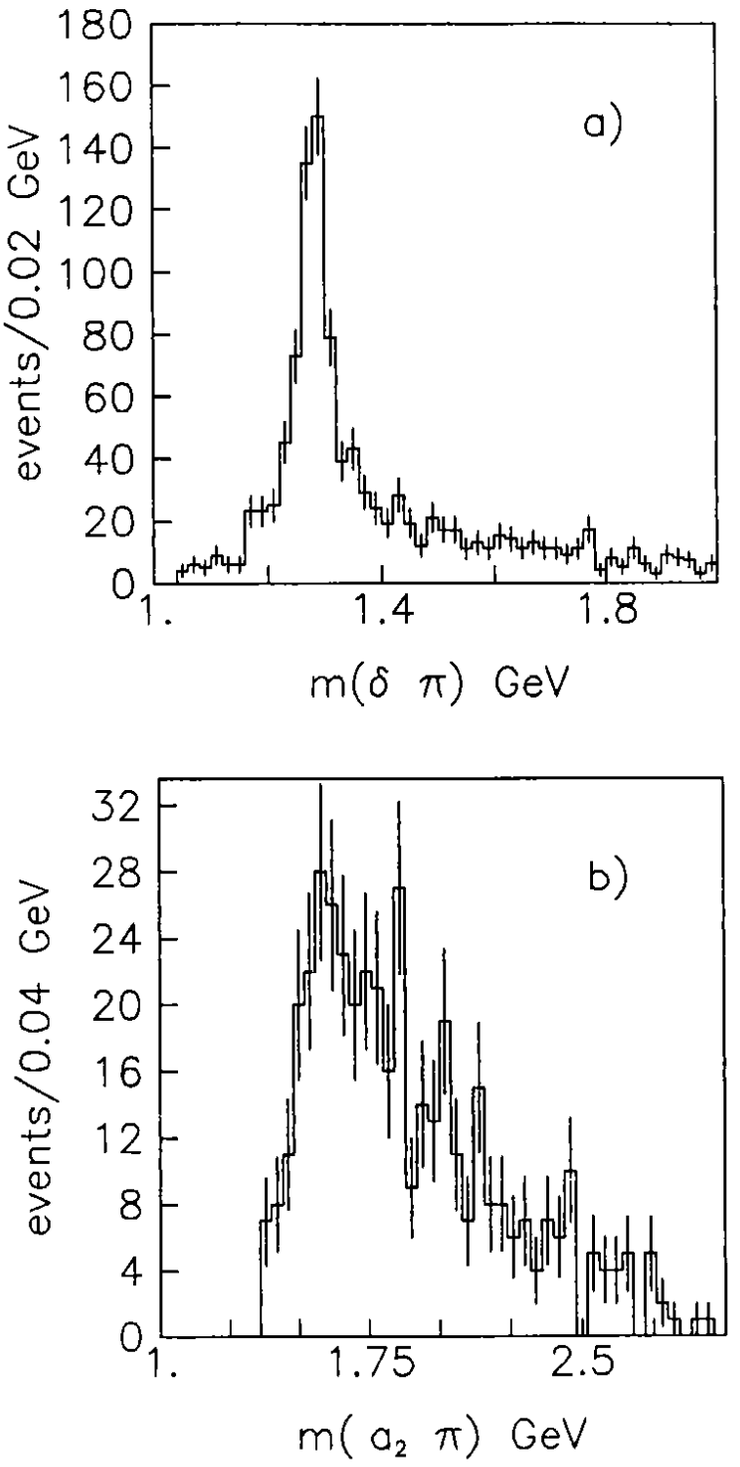
a)
events/0.02 GeV
180
160
140
120
100
80
60
40
20
0
1.
1.4
1.8
m(δ π) GeV
b)
events/0.04 GeV
32
28
24
20
16
12
8
4
0
1.
1.75
2.5
m(a2 π) GeV

Fig. 9

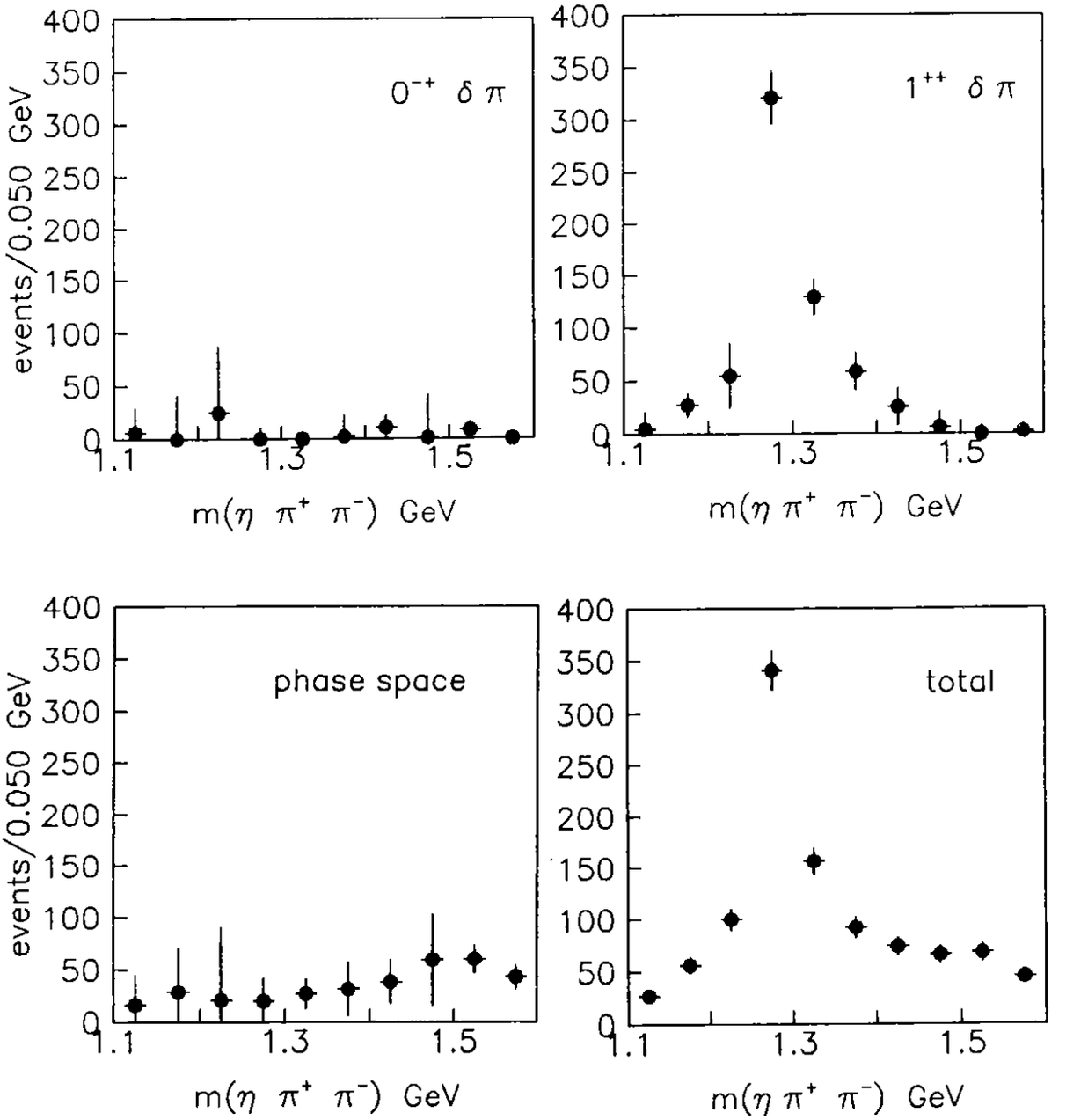
0^{-+} $\delta\,\pi$
1^{++} $\delta\,\pi$
phase space
total
events/0.050 GeV
$m(\eta\ \pi^+\ \pi^-)$ GeV
0
50
100
150
200
250
300
350
400
1.1
1.3
1.5

Fig. 10

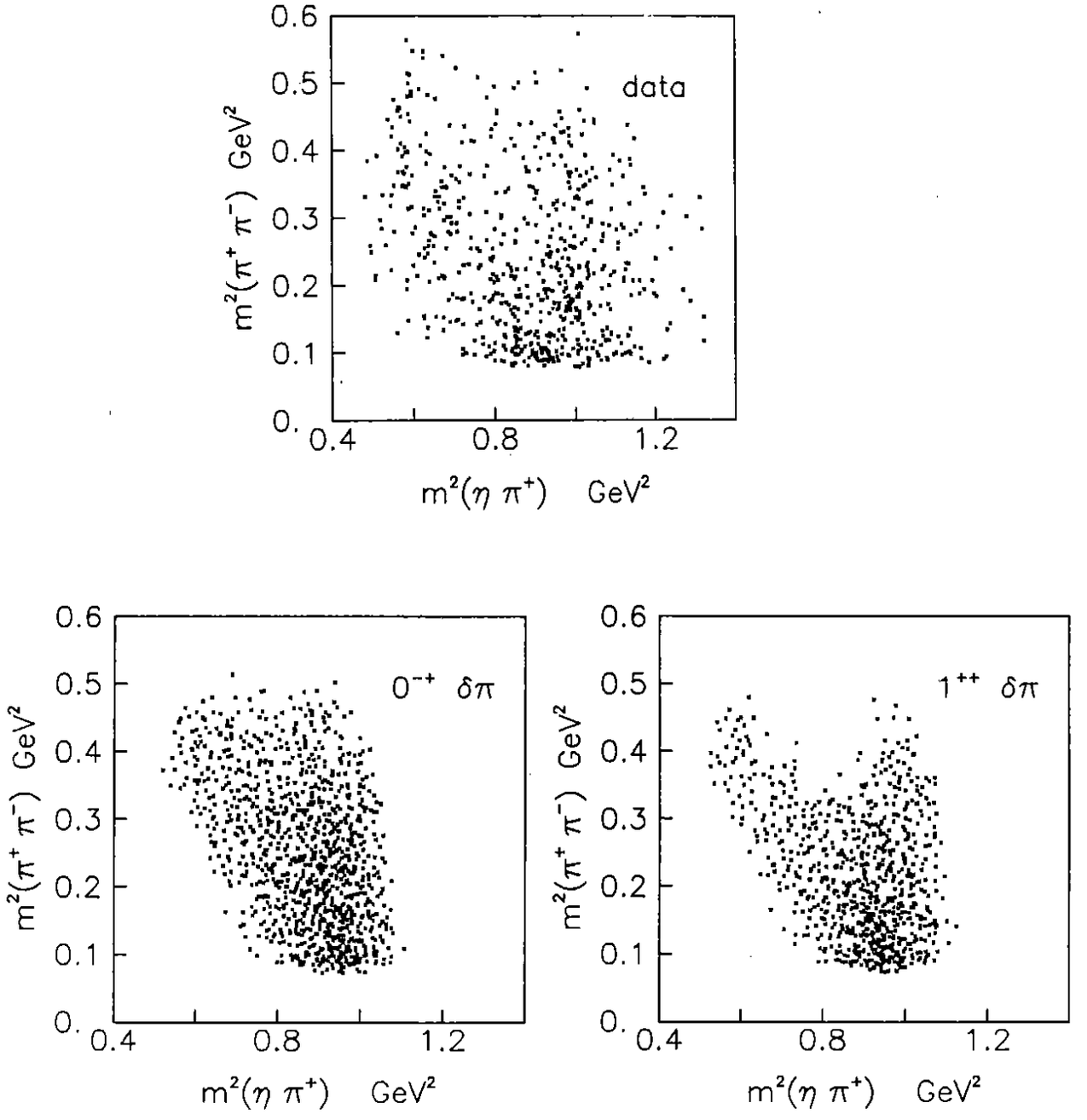
data
0^{-+} $\delta\pi$
1^{++} $\delta\pi$
$m^2(\pi^+\pi^-)$ GeV^2
$m^2(\eta\,\pi^+)$ GeV^2
0.6
0.5
0.4
0.3
0.2
0.1
0.
0.4
0.8
1.2

Fig. 11

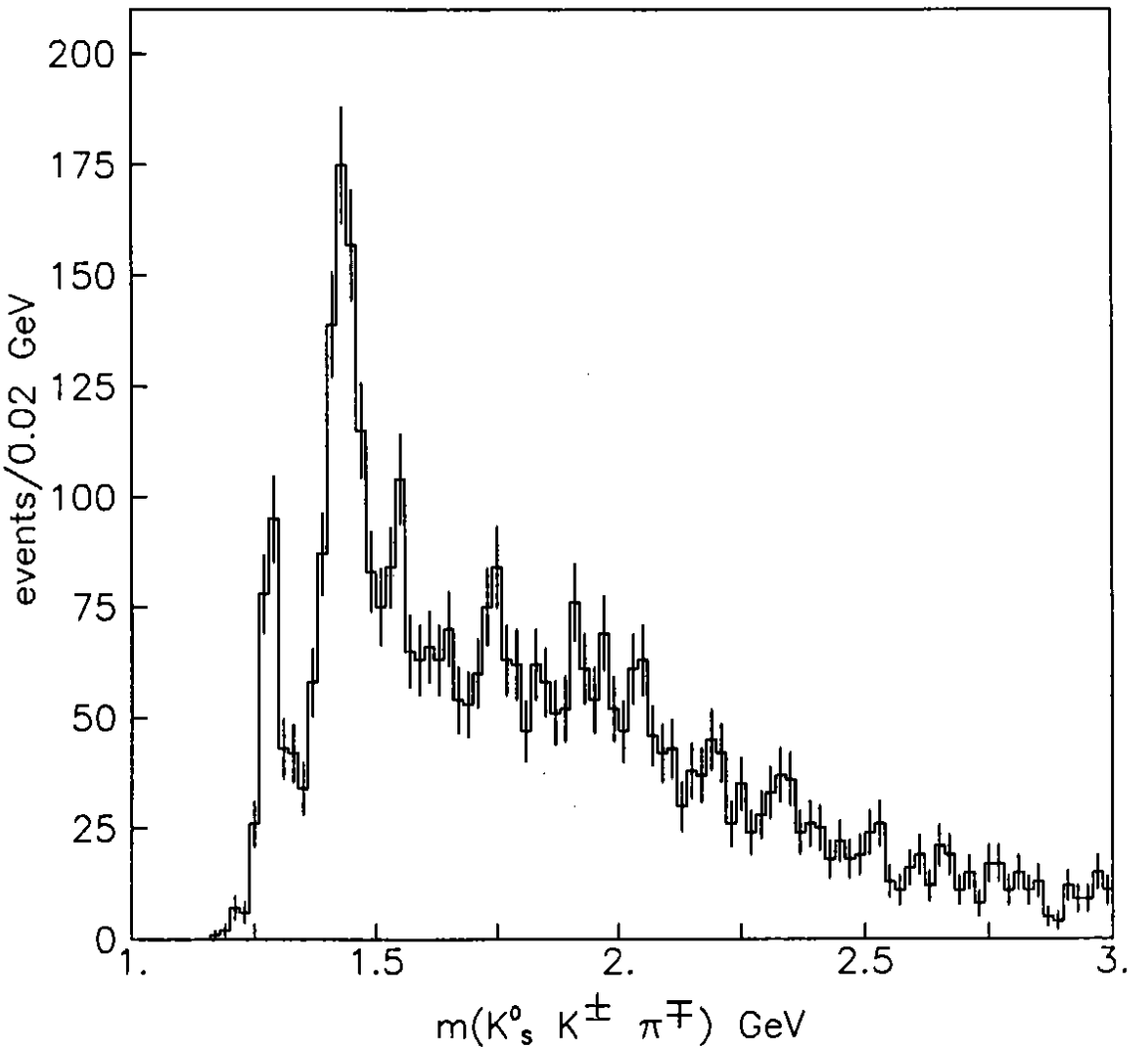

Fig. 12

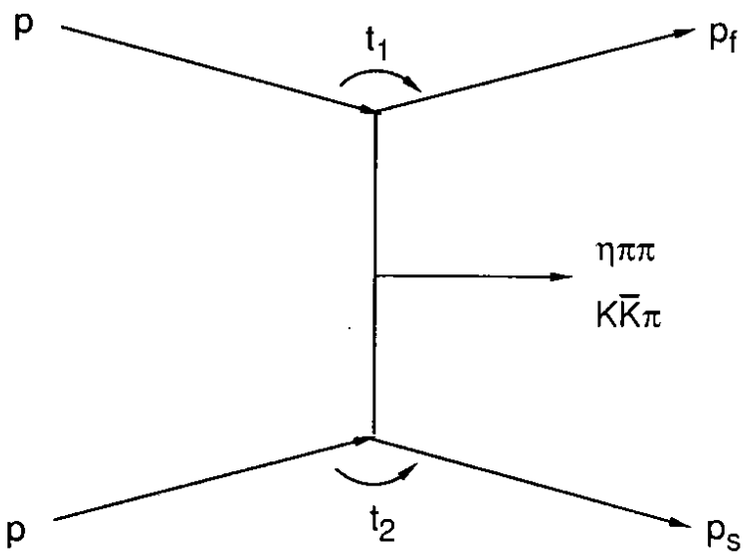

Fig. 13

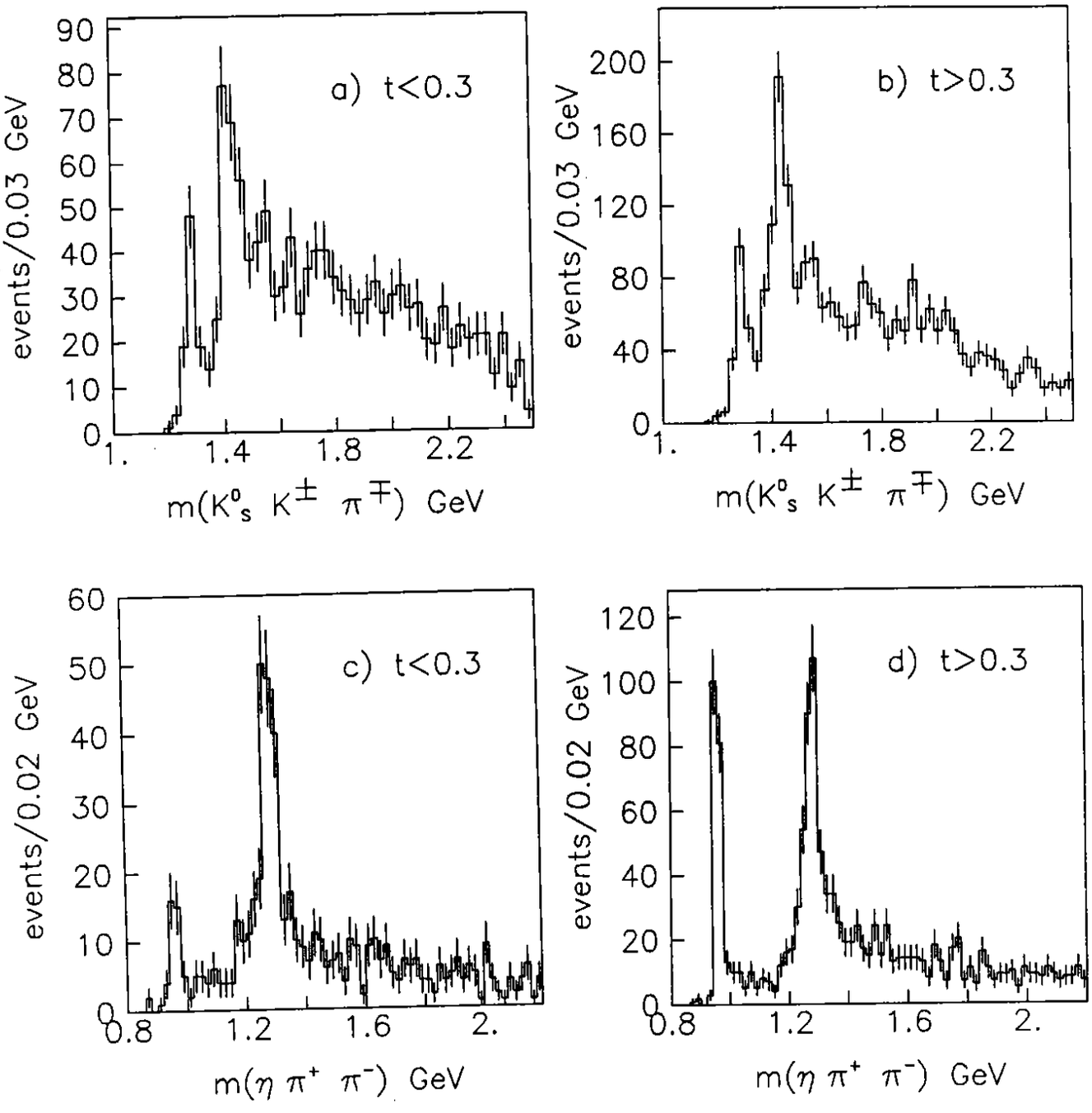
a) t<0.3
b) t>0.3
c) t<0.3
d) t>0.3
events/0.03 GeV
events/0.02 GeV
m(K⁰s K± π∓) GeV
m(η π⁺ π⁻) GeV

Fig. 14

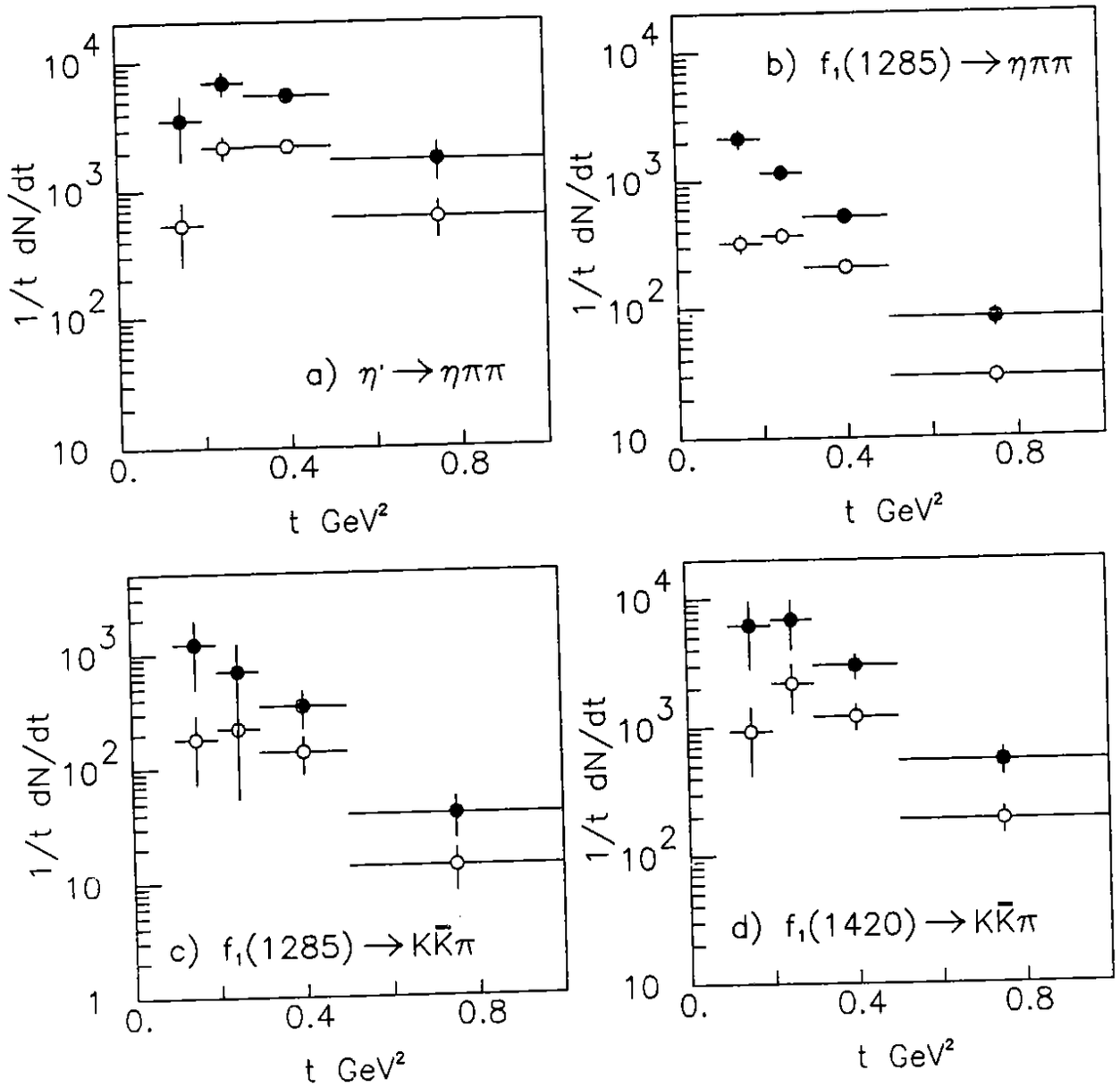

Fig. 15

Imprimé au CERN. Prix: 0.80 Fr.